Korean J. Chem. Eng., 39(11), 2945-2958 (2022)
DOI: 10.1007/s11814-022-1163-7

pISSN: 0256-1115
eISSN: 1975-7220

Bubble behavior and nucleation site density in subcooled flow boiling using a novel method for simulating the microstructure of surface roughness

Hasan Alimoradi*, Mehrzad Shams*,†, and Nasser Ashgriz**

*Multiphase Flow Lab, Faculty of Mechanical Engineering, K.N. Toosi University of Technology, No. 17, Pardis St., Mollasadra Ave., Vanak Sq., Tehran 19395-1999, Iran
**Department of Mechanical and Industrial Engineering, University of Toronto, 5 King's College Road, Toronto, ON M5S 3G8, Canada
(*Received 27 August 2021 • Revised 20 March 2022 • Accepted 28 April 2022*)

Abstract−The wall boiling model in the current research is used to predict the bubble dynamics treatment in flow boiling in a vertical pipe. A random surface roughness is developed for simulating the surface roughness effects in subcooled flow boiling as a novel method. This novel method is called direct roughness simulation (DRS). The DRS results are compared to the smooth surface (SS) and surface roughness model (SRM). The SRM is the traditional way of simulating surface roughness. The finite volume methods and Euler-Euler are applied to investigate subcooled flow boiling. The turbulence stresses are simulated by the k-ε model. The surface roughness effect on bubble dynamics for flow boiling is investigated numerically. According to the numerical simulations, nucleation site density is only increased by augmentation of heat flux. In contrast, increasing surface roughness, pressure, mass flux, and subcooled temperature cause a drop in nucleation site density. The bubble detachment waiting time and bubble departure diameter increase with the rise in pressure; however, by increasing other boundary conditions, these two parameters decrease. Results show that the reduction in the nucleation site density at outlet was 28.05% for the DRS and 25.5% for the SRM compared to the SS. The bubble detachment frequency at oulet 2.04% decreases when using the SRM and 6.5% increases when using the DRS.Compared to the SS; the bubble departure diameter at outlet 4.3% increases when using the SRM and 11.8% decreases when using the DRS.

Keywords: Bubble Dynamics, Subcooled Flow Boiling, Surface Roughness, Direct Roughness Simulation

INTRODUCTION

There is a high demand for novel methods to generate and use energy efficiently. The new methods and devices are also used to develop renewable energies such as fuel cells and solar cells. On the other hand, efficient system utilization depends on the in-depth study of related physical phenomena [1-3]. One of the challenges heat transfer researchers have been working on was finding a way to transfer or dissipate the heat with heat transfer and efficiency enhancement to improve the performance of the systems. The boiling phenomena help the researchers in this matter as the heat transfer coefficient of boiling is high. So it is used for cooling and heat absorption systems. It led to the study of the physics and parameters that affect the boiling heat transfer.

The high-performance heat exchangers considerably reduce energy utilization and have a significant environmental and economic impact. Flow boiling exists in various industries such as oil and gas refineries, power production, cooling, and refrigeration systems. Wall surface nucleation is defined as the vapor phase production of superheated liquid in tiny cavities on a heated surface. The vapor formed in nucleation sites is trapped in the microscopic roughness on the heated surface, providing sufficient energy to produce a bubble. So, bubble growth onset is dependent on the heat transfer in the tiny cavities. When the gas phase generation starts, the bubble grows quickly until reaching the bubble departure diameter. It is dependent on the pressure rise that happens due to surface tension in the interface of vapor-liquid phases. Then, the bubble grows because of the layer of the superheated temperature of liquid near the wall surface or leaves the nucleation site, or condenses into the bulk fluid. In boiling heat transfer systems, studying the fluid dynamics of boiling at the heated surface has significant importance. While the characteristics of the wall nucleation, such as bubble departure, are classic heat transfer phenomena, they need to be studied in a wide range of complex applications. For example, nucleate boiling is an effective method of transferring heat from hot surfaces, common in the cooling of electronic systems [4-8]. Moreover, with the recent surge in computational power and the significance of high-resolution multi-phase flow simulation, bubbles produced in subcooled flow boiling are critical, as nucleated bubbles show the boundary of the gas phase. The gas phase distribution within the two-phase flow cannot be precisely calculated without a deep comprehension of the gas phase generated from the heated boundary using the CFD simulations. It is the limiting element in the current capability of subcooled boiling simulations [9].

This limitation originates from the interfacial area concentration in Eulerian-Eulerian modeling by the two-fluid model. The phases

†To whom correspondence should be addressed.
E-mail: shams@kntu.ac.ir

are solved distinctively in the two-fluid model, solving the set of mass, momentum, and energy balance equations. Hence, the two phase interaction is calculated in the total six balance equations: three for each fluid phase, via interfacial transfer terms such as interfacial heat transfer, interfacial shear, interfacial drag, interfacial mass transfer, etc. These interfacial transfer terms define the degree of phase coupling modeled based on the driving forces and the interfacial area concentration [10]. The most critical parameter affecting subcooled flow characteristics such as boiling bubble density and the interfacial area concentration is wall nucleation, as it produces numerous tiny bubbles [4]. Wall nucleation is substantially dependent on the total concentration of interfacial area, which shows the significance of the source term of wall nucleation in the equation of interfacial area transport. It evaluates the concentration growth of the interfacial area in the two-phase flow [10].

The number of sites formed on the surface wall shows the nucleation site density that dynamically nucleates bubbles, and many researchers have significantly worked on it [11-18]. However, there is a significant lack in the study of bubble detachment diameter and bubble detachment frequency [4,7,19]. In flow boiling, convective effect is essential since additional forces are applied to the nucleating bubble by the liquid flow [6]. In recent years, researchers have expanded their research on the effects of the surface parameters in the flow boiling heat transfer both experimentally and numerically. Parahovnik and Peles [20] experimentally studied bubble dynamics in critical pressure of a subcooled flow boiling of carbon dioxide. They observed that the bubble diameter is decreased when the fluid is near critical pressure. Bhati et al. [21] numerically investigated the bubble growth time, bubble waiting time, and bubble departure diameter. They concluded that Unal correlation for bubble departure is capable of modeling the flow in low heat fluxes. Mukherjee et al. [22] proposed a novel numerical scheme using the lattice-Boltzmann model to investigate the bubble dynamics of subcooled flow boiling. Their numerical scheme was able to appropriately model the nucleation site densities compared to the Eulerian approach. They also studied the effects of wall superheat temperature and surface wettability on bubble characteristics. Khoshnevis et al. [23] studied the bubble departure diameter and bubble detachment frequency in the subcooled flow boiling using the Euler-Euler method.

Alimoradi et al. [24] obtained the optimal point in subcooled flow boiling so that wall surface temperature is minimum and vapor volume fraction is maximum. To reach this goal, they used an artificial neural network and multi-objective genetic algorithm. Continuing the previous work, they simulated boiling of the nanofluid and observed the effect of nanoparticles and different cross-sectional areas on heat transfer and bubble dynamics of the boiling phenomena using the Euler-Mixture approach [25-27]. In addition, they investigated experimentally surface roughness effects on pool boiling heat transfer by considering nanofluid. They showed that pool boiling heat transfer increases by increasing wall surface roughness [28]. They carried out transient simulations to investigate this phenomenon on the surface of the heater using the Eulerian-Eulerian method. The impacts of frequency and amplitude of oscillation, and heat flux on parameters like vapor volume fraction, the velocity of nanofluid, and HTC were examined. They found that applying the mechanical vibration led to an increase of up to 30.11% and 17.5% in the rate of heat transfer for larger amplitude and frequency of vibrations, in turn [29,30]. Chen et al. [31] experimentally studied subcooled flow boiling of R-134a in a horizontal channel. They studied the effect of heat flux oscillation on bubble dynamics. The results disclosed that bubble dynamics would also fluctuate as the heat flux changes. They investigated the impact of vibration on the boiling characteristics of the silica nanofluid (0.01% vol) on a horizontal flat surface. Mohammed et al. [32] investigated nanofluid boiling in tubes located horizontally in a porous medium. They employed metal foams that had high conductivity to improve the boiling heat transfer rate in the computational zone. The mixture model was used to model R134a and ZnO nanofluid characteristics in the boiling process. They found that the utilization of metal foam caused an increase in the amount of vapor volume fraction and HTC at the outlet of the pipe. Moreover, a higher pressure loss was reported which was mainly due to the resistance of the flow caused by the creation of the porous medium. And they developed a model to determine the heat and mass transfer in the duct of a boiler using a commercial CFD code. They carried out numerical simulations to evaluate the impact of nanofluid concentration, the velocity of the fluid, as well as temperature of the boiler on the boiling characteristics of the whole system using mixture model. They also investigated the behavior of the system when one of the components evaporated. They found that vapor volume fraction and the HTC at the outlet increased when the concentration of the nanoparticle was increased [33]. Anotherwork [34] studied the effect of nanofluid concentration, flow rate, and the temperature of the boiler on the solution of the acetone and zinc bromide in a rectangular channel experimentally. They found that the Rohsenow constant in the boiling correlation for acetone/ZnBr2 nanofluid was 0.217 on the stainless steel surface. When the nanoparticle loading increased, the steady pressure in the system increased, leading to the enhancement of the temperature. As well as another study [35] investigated the phase change behavior of the acetone in the condenser and evaporator numerically to find the enhancement rate of the components in the whole system. The combination of the VOF and mixture models was utilized to study condensation and evaporation of this fluid in a circular tube located horizontally in the system. The temperature and the velocity of the fluid changed to investigate the impact of such parameters on the evaporation and condensation process. The results indicated that during the evaporation process, the HTC increased when the temperature and velocity difference between the wall and inlet went up. They also found that when the condensation rate increased, the stock of liquid in the evaporator increased, which showed that the rate of evaporation improved in the whole system.

In our previous study, the wall surface roughness effects on the heat transfer characteristics were investigated [8]. However, the surface roughness effect on bubble dynamics has not been investigated in this manner yet. In the subcooled flow boiling, a novel scheme for simulating the wall surface roughness is introduced named direct roughness simulation. In the current study, an evaluation of the effects of the microstructure on bubble dynamics (i.e., nucleation site density, bubble departure diameter, bubble detachment frequency, and bubble detachment waiting time) was done.

In order to fully understand the effect of roughness, a thorough study of roughness models was carried out. The proposed model of DRS was compared with the conventional SRM and smooth surface. Furthermore, operational conditions variations can influence the bubble dynamics; hence, a precise study of these parameters and their effects on the bubble dynamics with the DRS was done.

NUMERICAL METHODOLOGY

Using the Euler-Euler method, the set of mass, momentum, and energy conservations equations was solved for each fluid phase. The water is the continuous phase, and the vapor is the dispersed phase. For a more thorough explanation of the Euler-Euler numerical approach, the reader is referred to our previous work [24].

The numerical governing equations are continuity, momentum and energy conservations. In the following, the mentioned equations are brought for liquid and vapor phase.

$$\frac{\partial(\rho_l\alpha_l)}{\partial t}+\nabla\cdot(\rho_l\alpha_l\mathbf{u}_l)=\Gamma_{lg} \tag{1}$$

$$\frac{\partial(\rho_g\alpha_g f_i)}{\partial t}+\nabla\cdot(\rho_g\alpha_g\mathbf{u}_g)=S_i-f_i\Gamma_{lg} \tag{2}$$

$$\frac{\partial(\rho_l\alpha_l\mathbf{u}_l)}{\partial t}+\nabla\cdot(\rho_l\alpha_l\mathbf{u}_l\mathbf{u}_l)=-\alpha_l\nabla P+\alpha_l\rho_l\mathbf{g} +\nabla[\alpha_l\mu_l^e(\nabla\mathbf{u}_l+(\nabla\mathbf{u}_l)^T)]+(\Gamma_{lg}\mathbf{u}_g-\Gamma_{gl}\mathbf{u}_g)+F_{lg} \tag{3}$$

$$\frac{\partial(\rho_g\alpha_g\mathbf{u}_g)}{\partial t}+\nabla\cdot(\rho_g\alpha_g\mathbf{u}_g\mathbf{u}_g)=-\alpha_g\nabla P+\alpha_g\rho_g g +\nabla[\alpha_g\mu_g^e(\nabla\mathbf{u}_g+(\nabla\mathbf{u}_g)^T)]+(\Gamma_{gl}\mathbf{u}_l-\Gamma_{lg}\mathbf{u}_g)+F_{gl} \tag{4}$$

$$\frac{\partial(\rho_l\alpha_l H_l)}{\partial t}+\nabla\cdot(\rho_l\alpha_l\mathbf{u}_l H_l)=\nabla[\alpha_l k_l^e(\nabla T_l)]+(\Gamma_{gl}H_l-\Gamma_{lg}H_g) \tag{5}$$

$$\frac{\partial(\rho_g\alpha_g H_g)}{\partial t}+\nabla\cdot(\rho_g\alpha_g\mathbf{u}_g H_g)=\nabla[\alpha_g k_g^e(\nabla T_g)]+(\Gamma_{lg}H_g-\Gamma_{gl}H_l) \tag{6}$$

Mass transfer parameters are calculated by:

$$\Gamma_{lg}=\frac{h a_{if} T_{sub}}{h_{fg}} \tag{7}$$

$$\Gamma_{gl}=\frac{Q_e}{h_{fg}} \tag{8}$$

MATHEMATICAL MODELING

1. Governing Equations

Sensible heat is the heat flux given to the fluid to reach the saturated point, and latent heat is generated vapor using wall heat flux. The sensible heat is simulated by turbulent convection, while periodical bubble generation induces fluid mixing in turbulent convection. The mentioned induced fluid mixing is called "quenching". It is used to model the effects of transient conduction generated by the patches of colder fluid replacing departed bubble from the surface wall. The wall heat flux includes convective heat flux, quenching, and evaporation [8]:

$$Q_{tot}=Q_c+Q_{tc}+Q_e \tag{9}$$

where Q_c is convective heat flux, Q_{tc} is quenching, and Q_e is evaporation.

There are three different heat fluxes. They are introduced by convective heat flux for liquid, evaporation for phase changing from liquid to gas, and quenching heat fluxes for stagnant bubbles on the wall. Eqs. (10)-(12) explain turbulent convection heat flux [24].

$$Q_c=A_{1f}\frac{\rho_L C_{pl}\mathbf{u}_l}{T^+_{y^+(L)}}(T_W-T_l) \tag{10}$$

$$A_{1f}=1-A_{tc} \tag{11}$$

$$A_{tc}=\min\left(\pi\frac{(a d_W)^2}{4},\,1\right) \tag{12}$$

In Eq. (10), a non-dimensional temperature is illustrated by $T^+_{y^+(L)}$. As Eq. (12) a is the bubble influence factor whose value is two. Also, ρ_l, C_{pl}, $\mathbf{u}_l$, T_W, T_l, and d_W are liquid density, liquid specific heat, velocity of liquid, wall temperature, liquid temperature, and bubble departure diameter, respectively.

Eq. (13) demonstrates the evaporation heat flux. The vapor mass flux is shown $\dot{m}_W$ that is produced by bubbles formed within active nucleation sites. h_{fg} is the specific enthalpy change. As per Eq. (14), the vapor mass flux is determined [24]. In Eq. (6), ρ_g, N_a, and f are vapor density, nucleation site density, and bubble departure frequency.

$$Q_e=\dot{m}_W h_{fg} \tag{13}$$

$$\dot{m}_W=\rho_g\frac{2}{3}\frac{d_w}{a^2}A_{tc}N_a f \tag{14}$$

The conductive heat transfer involves the heat transfer for a stagnant bubble on the wall surface. The heat transfer between the wall and fluid is identified as transient heat transfer by [24].

$$Q_{tc}=\left(\frac{2}{\sqrt{\pi}}\sqrt{k_l\rho_l C_{pl} f}\right)A_{tc}(T_w-T_l) \tag{15}$$

where k_l is the liquid conductivity. The saturation temperature in the subcooled flow boiling is more than the bulk temperature of the fluid in the local pressure. The fluid temperature near the wall surface is enhanced due to heat flux and onset nucleate boiling occurs when its wall surface temperature is more than the saturated temperature. Then bubble formation starts on the wall surface of the pipe, which is named nucleation sites. When the evaporation rate is increased, bubbles are larger. They depart from the hot surface wall when they attain their maximum diameter. Eq. (16) is applied to determine active nucleation site density [36]:

$$N_a=(185\Delta T_{sup})^{1.805} \tag{16}$$

The bubble departure frequency is approximated by Eq. (17) [37]:

$$f=\sqrt{\frac{4g(\rho_l-\rho_g)}{3d_w\rho_l}} \tag{17}$$

When the bubble is departed from the surface wall, it reaches a specific diameter. This diameter is named bubble departure diameter. The bubble departure diameter is a useful parameter in the study of bubble dynamics on nucleate boiling. Eq. (18) is applied for obtaining the bubble departure diameter [38]:

$$d_w = \min\left(0.6\exp\left(\frac{-\Delta T_{sub,Lw}}{45}\right), 1.4\right) \quad (18)$$

Since a bubble is separated from the surface wall, another bubble in this position (the same nucleation site) is produced. This period between departure and production of the bubble is called the waiting time. Waiting time in the present study is measured by Eq. (19) [39]:

$$t_w = \frac{0.8}{f} \quad (19)$$

More information about the governing equation was discussed in our previous work [8]. Ansys CFX code was utilized to solve the governing equations of pool boiling presented in Eq. (1) to Eq. (19) numerically. The popular y^+ is used in this study in order to improve the results in evaluating the logarithmic layer. The y^+ is set to 250 among all other possible choices. This model is implemented in Ansys CFX, and it is fixed to the near-wall grid cell size in a wide range. By using y^+ not only heat and mass transfer modeling is improved but also the velocity wall function grids are simulated adequately [8]. Furthermore, this model is used in similar studies, [40,41], and accurate results are derived.

2. Boundary Conditions

Mass flow rate, pressure, and constant heat flux, and no-slip condition are assumed at the inlet, outlet, and wall, respectively, as the boundary conditions [42,43]. Since these two studies are two of the very successful studies in the field, they have been used for verifying the results from the numerical simulations.

DISCUSSION OF ROUGHNESS MODELS

1. Surface Roughness Model

The wall function of the near-wall fluid is changed using the SRM. In this model, the profile is logarithmic for the rough wall but closer to the wall than the smooth surface wall. Near-wall computations are more complex since they become dependent on two parameters: the height of roughness and the y^+. Wall roughness is the equal sand-grain roughness thickness, while the sand-grain roughness is not equivalent to the roughness geometric thickness of the surface wall. The wall friction relates to surface roughness thickness and the form of surface roughness. It is necessary to characterize the equivalent roughness thickness of sand-grain [44,45].

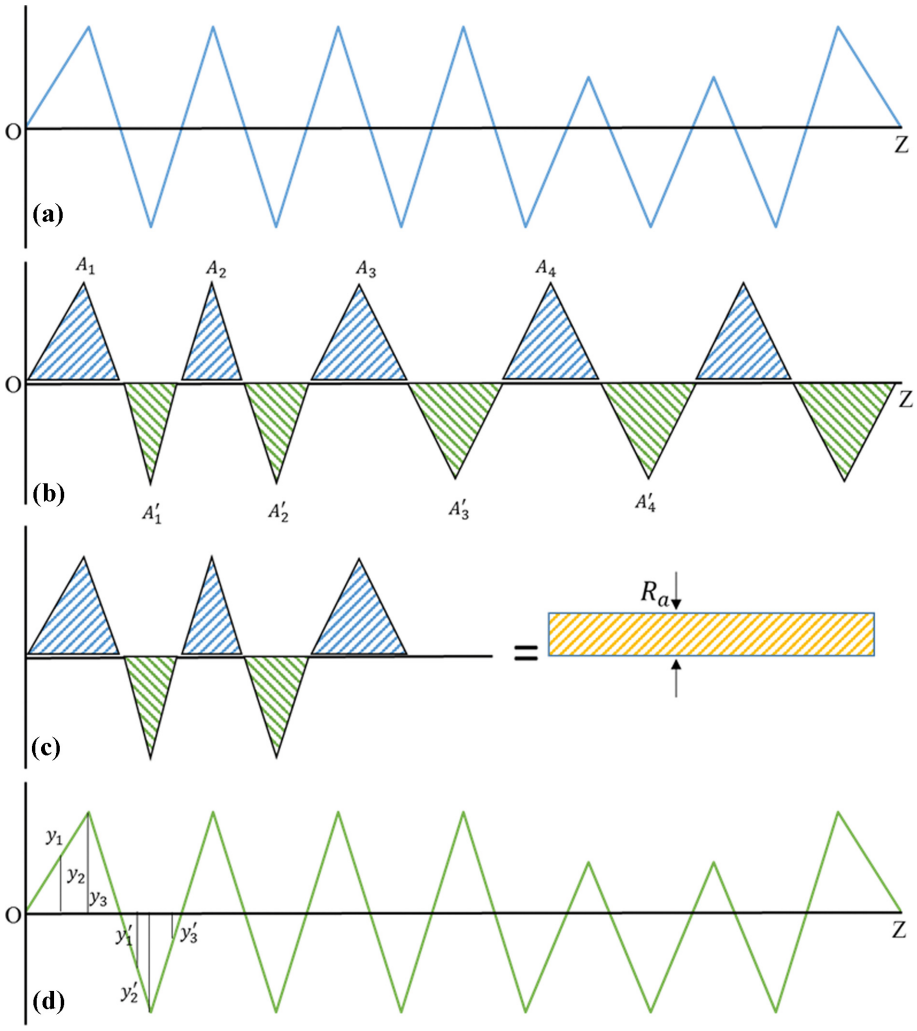

Fig. 1. Surface roughness modeling by direct roughness simulation.

2. Direct Roughness Simulation

In the present study, the novel scheme of DRS was utilized to simulate the surface roughness. The advantage of this method is in phase change modeling. This model is capable of simulating the turbulence, vortexes, and vapor volume fraction in cavities. The DRS model directly studies the surface roughness, and it is a novel method to model the boiling phenomenon in pores of rough surface. Aditionally, this method is able to model the vapor volume fraction as well as the turbulence in the pores.

DRS is a new model to determine the roughness by randomly finding the height of roughness. The mean surface roughness is taken as the baseline, the relative height is evaluated for further investigations. The peaks and pores create areas as in Fig. 1. The summation of areas higher and lower than the baseline must equal to zero [8].

$$A=A_1+A_2+A_3+\cdots=A_1'+A_2'+A_3'+\cdots \tag{20}$$

The surface roughness, R_a, is the average of the peaks and pores, as shown in Fig. 1(b). As shown in Fig. 1(a), the OZ line is the average line for the peaks and pores. This line is carefully drawn where the summation of the area above and below this line is zero. If the set of the A_n and A_n' surfaces is shown as A, then A can be shown as a strip with the length of OZ and constant width, as shown in Fig. 1(c). This is similar to the R_a (the average roughness). Fig. 1(d) depicts the number of positive heights y_1, y_2, y_3 and … is the same as the negative heights y_1', y_2', y_3' and … n R_a is calculated as Eq. (13) in which n is the number of the peaks.

$$R_a=\frac{y_1+y_2+y_3+\cdots+|y_1'|+|y_2'|+|y_3'|+\cdots}{2n} \tag{21}$$

In order to increase the accuracy, all the surfaces are divided to L.

$$R_a=\frac{\text{integral of the surfaces}}{L} \tag{22}$$

The behavior of the fluid between the pores of the rough surface cannot be simulated by the SRM. The DRS model can be simulated the roughness physically, fluid behavior, bubble dynamic and the local phase change between the pores.

NUMERICAL VALIDATION

1. Smooth Surface Validation

The experimental data for validating the numerical results of the smooth surface of subcooled flow boiling are used by the experiments of Bartolome et al. [43]. Table 1 shows the operational conditions of numerical simulation.

The simulation and validation results are shown in Fig. 2. Results show that average water temperature, average vapor volume fraction, and wall surface temperature agree with experimental data. The onset of nucleate boiling of simulation results is compared with experiments showing that they are well compatible.

Table 1. The operational conditions for validating simulation results of SS

Validation case	Subcooled temperature (K)	Heat flux (kW/m^2)	Pressure (MPa)	Mass flux (kg/m^2s)	Section/Diameter (cm)
(1) [43]	58.2	570	4.5	900	diameter=15.4

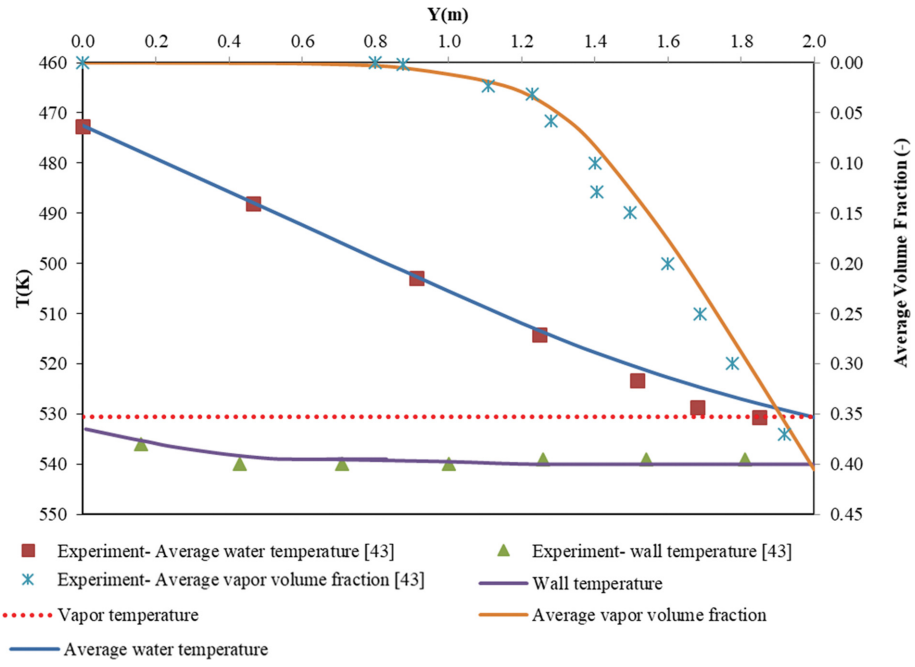

Fig. 2. Average bulk temperature, average vapor volume fraction, and wall surface temperature along the pipe.

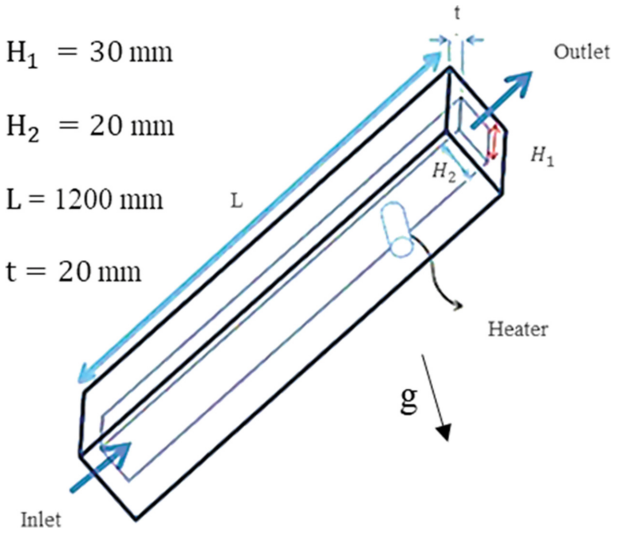

Fig. 3. Geometry of the channel.

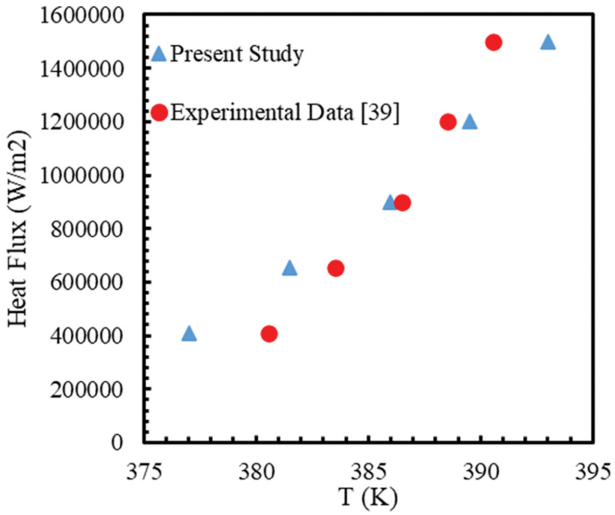

Fig. 4. Heat flux vs. wall surface temperature.

Table 2. Grid independency examination

Wall surface temperature (K)	Number of nodes
411.01	58,325
410.31	60,823
410.01	61,145

2. Rough Surface Validation

2-1. Geometry and Grid Independence

The pure water subcooled flow boiling is presented with a rectangular cross-section in a horizontal channel, similar to the experimental investigation of Setoodeh et al. [46]. The heat flux is produced by a heater close to the bottom of the channel surface, a 12 mm diameter circular plate, as shown in Fig. 3. The gravity direction is in the direction of the heater. The geometric features of the channel are displayed by H_1, H_2, L, and t in Fig. 3.

The boundary conditions at these locations--heater surface, other walls, inlet, and outlet--are heat flux, adiabatic, fluid velocity, and relative pressure.

The grid independence is shown in Table 2 for three node numbers for the average wall surface temperatures. Since the wall surface temperature is negligible enough, the second case is selected for the number of nodes.

The boundary conditions are the ones in Setoodeh et al. experiments [39]. The surface roughness, the temperature at the inlet, pressure, and the fluid velocity at the inlet are 4.5 μm, 353 K, and 1.2 bar, 0.9 m/s, respectively. To capture the surface roughness, the surface roughness model has been used. The heat flux versus wall surface temperature is indicated in Fig. 4. It is observable that the numerical results with the experiments match well. At heat flux at 400,000 W/m^2, because the onset nucleate boiling is started, the difference value between the numerical simulation and experimental result is greater. As the higher heat fluxes approach, the experimental results and numerical simulation results are well compatible. Therefore, in the continuation of the paper, numerical simulations in the range of medium to high heat fluxes of 0.6 to 1 MW/m^2 are performed, which are in the appropriate range in terms of validation.

GEOMETRY AND GRID INDEPENDENCE OF DRS

The surface roughness geometry is generated for the simulations by a random surface microstructure shown in Fig. 5(a). This method of surface roughness modeling is named DRS. The average wall surface roughness is R_a=50 μm. A vertical pipe is considered with a length of 20 cm and its 5° circular sector. The diameter of the pipe is 15.4 mm as the flow cross-section.

Grid independence was investigated for three grids. The average vapor volume fraction and the wall surface temperature for different grids are shown in Fig. 5(b) and Fig. 5(c). The results represent that the differences between different node numbers are small, which shows the grid independence. The roughness was generated for ten different cases with random roughness so that the average roughness was about 50 μm. In all cases, the average wall surface temperature was approximately the same. Based on Fig. 5, the gird independence for 217,831 nodes was obtained.

The three grids are selected to verify the grid independence. The average vapor volume fraction in the outlet of the tube and average

Table 3. Grid independence for different node numbers

Number of nodes	Average vapor volume fraction at the outlet	Relative error vapor volume fraction at outlet %	Average wall temperature (K)	Relative error wall temperature (K) %
124,196	0.3583	-	558.408305152233	-
166,076	0.3599	0.444%	557.910288933855	0.089%
217,831	0.3608	0.25%	557.60530192452	0.054%

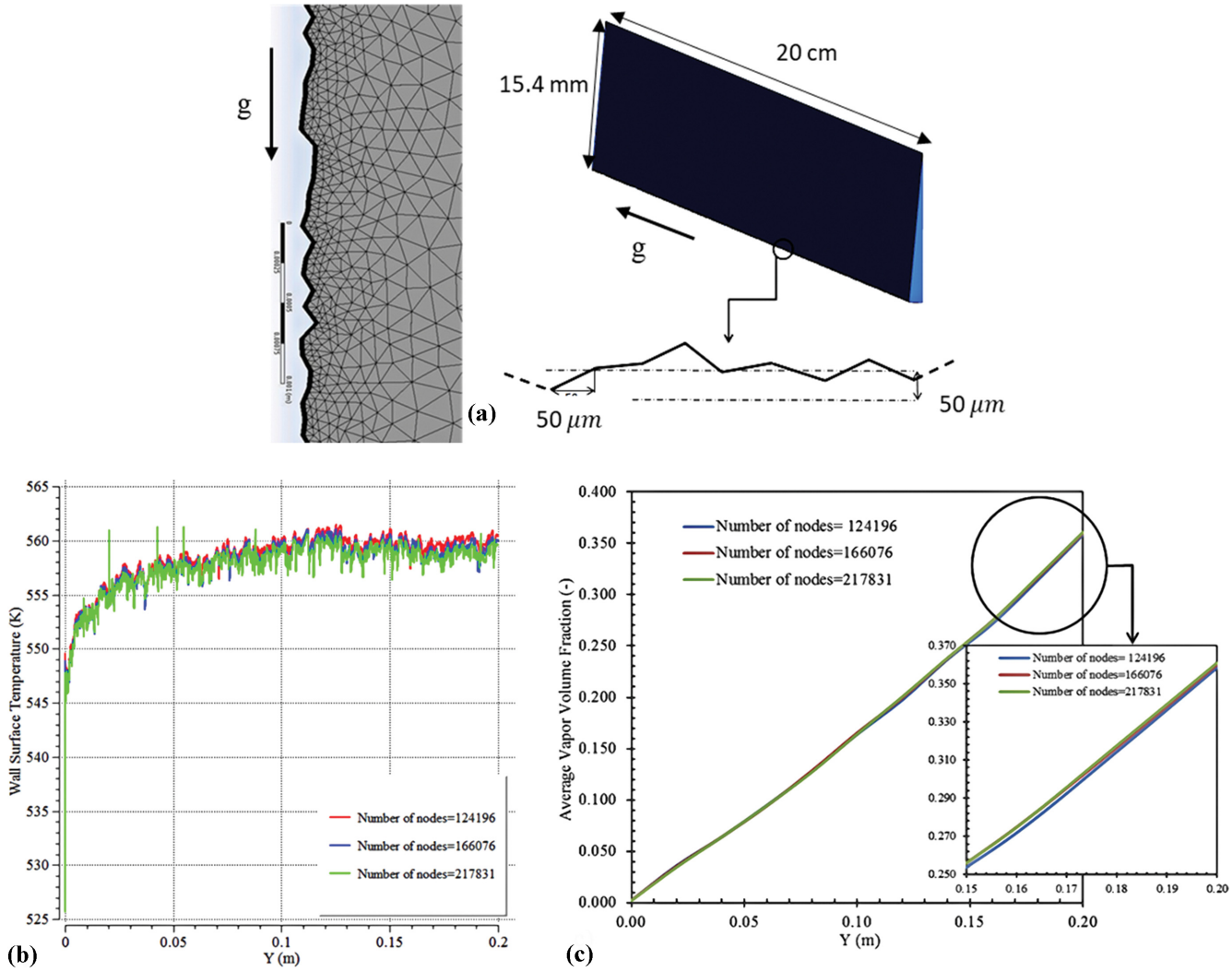

Fig. 5. The geometry and grid independence (a) geometry of the simulated pipe, (b) wall surface temperature, (c) average vapor volume fraction.

wall temperature along the tube for different grid sizes are shown in Table 3. It shows that the relative error for average vapor volume fraction and average wall temperature in grid independency of mesh are 0.25% and 0.054%, respectively. Based on the values of relative error, gird independence is achieved with 217,831 nodes.

RESULTS AND DISCUSSION

The bubble dynamics was studied for DRS, SRM, and SS. Results of DRS for bubble properties are presented for different operational conditions.

1. Bubble Properties

The nucleation process is determined in a pipe flow at 4.5 MPa, 0.8 MW/m^2, 600 kg/m^{2}s, and 5 K for pressure, heat flux, mass flux, and subcooled temperature, respectively. Fig. 6(a) shows the nucleation site density for three different surfaces: (i) a SS, (ii) a surface with the SRM, and (iii) a surface with DRS. Increasing the surface roughness decreases the nucleation site density. The results for the SRM are close to those with DRS. As the wall temperature in the rough condition varies and follows a vibrational behavior, the existence of cavities on the surface causes an enhancement in the number of nucleation site. The temperature inside the cavity increased since the heat inside the cavity was trapped, leading the bubbles to nucleate inside the cavity and the number of nucleation sites to increase. On the other hand, increasing the surface roughness brings about an increase in the wall surface area, which is heavily dependent upon roughness height. As the nucleation site density is derived from dividing the nucleation sites by hot surface area, the reduction in nucleation site density is mainly due to the further increase in hot surface area relative to the number of nucleation sites. So, this term was replaced with the previous term. However, between these two contributing factors for nucleation site density, surface roughness plays an important role, and thus, the total nucleation site density decreases. The surface roughness decreases the surface temperature, which affects the number of nucleation sites. So, the nucleation site density is increased in lower surface roughness cases compared to the SS, while it is decreased in higher surface roughness cases.

The bubble detachment frequency for the three surfaces is provided in Fig. 6(b). The bubble detachment frequency for the DRS

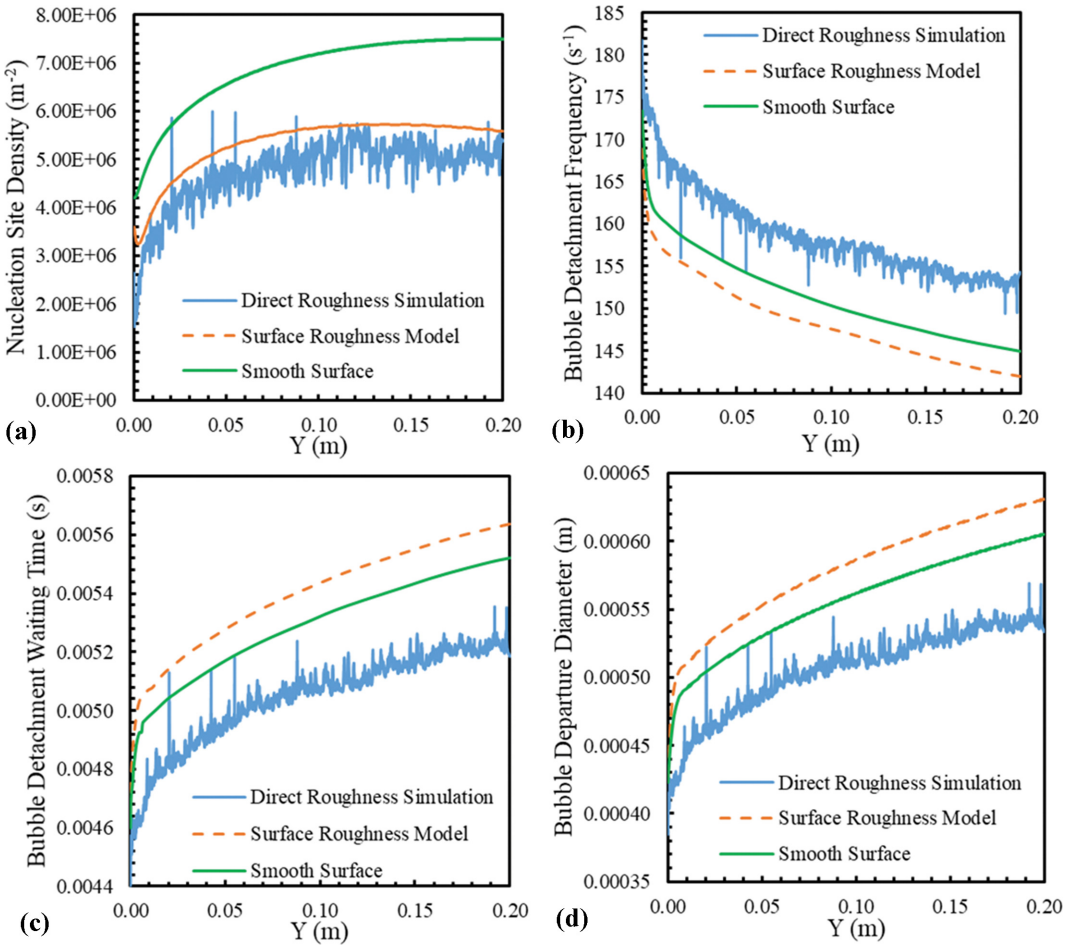

Fig. 6. Surface roughness effects on (a) nucleation site density, (b) bubble detachment frequency, (c) bubble detachment waiting time, (d) bubble departure diameter using DRS, SRM, and SS.

is more than that of the SS, which is more than that of the SRM. The surface roughness leads to more turbulence near the wall, which increases the bubble departure speed. The bubble detachment frequency depends on the detachment speed, and therefore, it increases as well. The bubble detachment frequency enhances heat transfer since the bubbles are detached with more frequency, and the liquid water replaces them. So, more heat is taken from the wall surface, which causes a decrease in the wall surface temperature and improvement of the heat transfer.

The bubble detachment waiting time is shown for the three surfaces in Fig. 6(c). The bubble detachment waiting time along the pipe for DRS is less than that of the SS, which is less than that of the SRM. The bubble detachment waiting time and bubble detachment frequency are inversely proportional. Therefore, higher bubble detachment frequencies result in shorter bubble detachment waiting time.

The bubble departure diameter is illustrated for the three surfaces in Fig. 6(d). The bubble departure diameter for the DRS is less than that for the SS, which is less than that for the SRM. This is related to the bubble detachment frequency and bubble detachment waiting time. As the attachment time of the bubble decreases, it has less time to grow so that it will have a smaller final diameter. By considering the work of Sarker et al. [47], bubble departure diameter decreases when the roughness increases, and as the bubble departure diameter decreases, bubble detachment frequency rises. This is in agreement with the results obtained by direct roughness simulation.

In flow boiling heat transfer, the decrease of the bubble departure diameter is a favorable factor. The surface roughness causes turbulence near the walls, which leads to faster detachment of the bubbles from the wall, and consequently, smaller bubble diameter. The bubble has a lower specific heat capacity as it is in the vapor phase. The larger bubbles play the role of an insulation layer that prevents heat transfer. So, the lower bubble departure diameter leads to a higher heat transfer coefficient.

The most critical parameter in the heat transfer of boiling is delaying the critical heat flux (CHF). When the CHF is reached, nucleate boiling is ended while the film boiling is started. Bubbles are created on the wall surface in nucleate boiling. The bubble coalescence causes to decrease heat transfer coefficient and CHF occurs. While the vapor bulks are merged, slug flow is formed in the film boiling. The slug flow reduces the heat transfer and increases the wall surface temperature, which leads to the burning of the wall surface. In the cases of rough surfaces, the roughness causes tur-

bulence near the heater wall surface, which leads to the increase of the bubble detachment frequency. It is a favorable factor as it leads to the lower bubble detachment diameter, which prevents the bubbles from merging and formation of the slug flow. So, the slug flow that is unfavorable for heat transfer is delayed, and the heat transfer is improved.

The smooth surface model was validated with the experimental work of Bartolomej et al. [43]. However, the surface roughness model was verified with the experimental results of Setoodeh et al. [46]. Moreover, by comparing the findings of direct roughness simulation with surfaced roughness model, we can conclude that both of the models predicted the surface temperature well [8]. On the other hand, the data obtained for bubble departure diameter and bubble detachment frequency from the direct roughness simulation model were qualitatively closer to the experimental results of Sarker et al. [47] compared to the smooth surface, in a way that applying the roughness, leading to an enhancement and decrease in bubble detachment frequency and bubble departure diameter, respectively, compared to the smooth surface. This result follows a similar trend to the experimental work of McHale et al. [48].

2. Effect of Pressure on Bubble Dynamics Using DRS

The bubble properties were determined for the heat flux of 1 MW/m^2, mass flux of 800 kg/m^{2}s, the subcooled temperature of 10 K, surface roughness 50 μm, and three different pressures of 1.5 MPa, 4.5 MPa, and 7 MPa. The pressure effects on the nucleation site density, bubble detachment frequency, bubble detachment waiting time, and bubble departure diameter are shown in Fig. 7. Fig. 7(a) shows that the nucleation site density decreases with increasing pressure. The nucleation site density is dependent on the wall superheat temperature. It is also related to the saturation temperature, which depends on the fluid pressure. The approximate superheat temperatures for pressures of 1.5 MPa, 4.5 MPa and

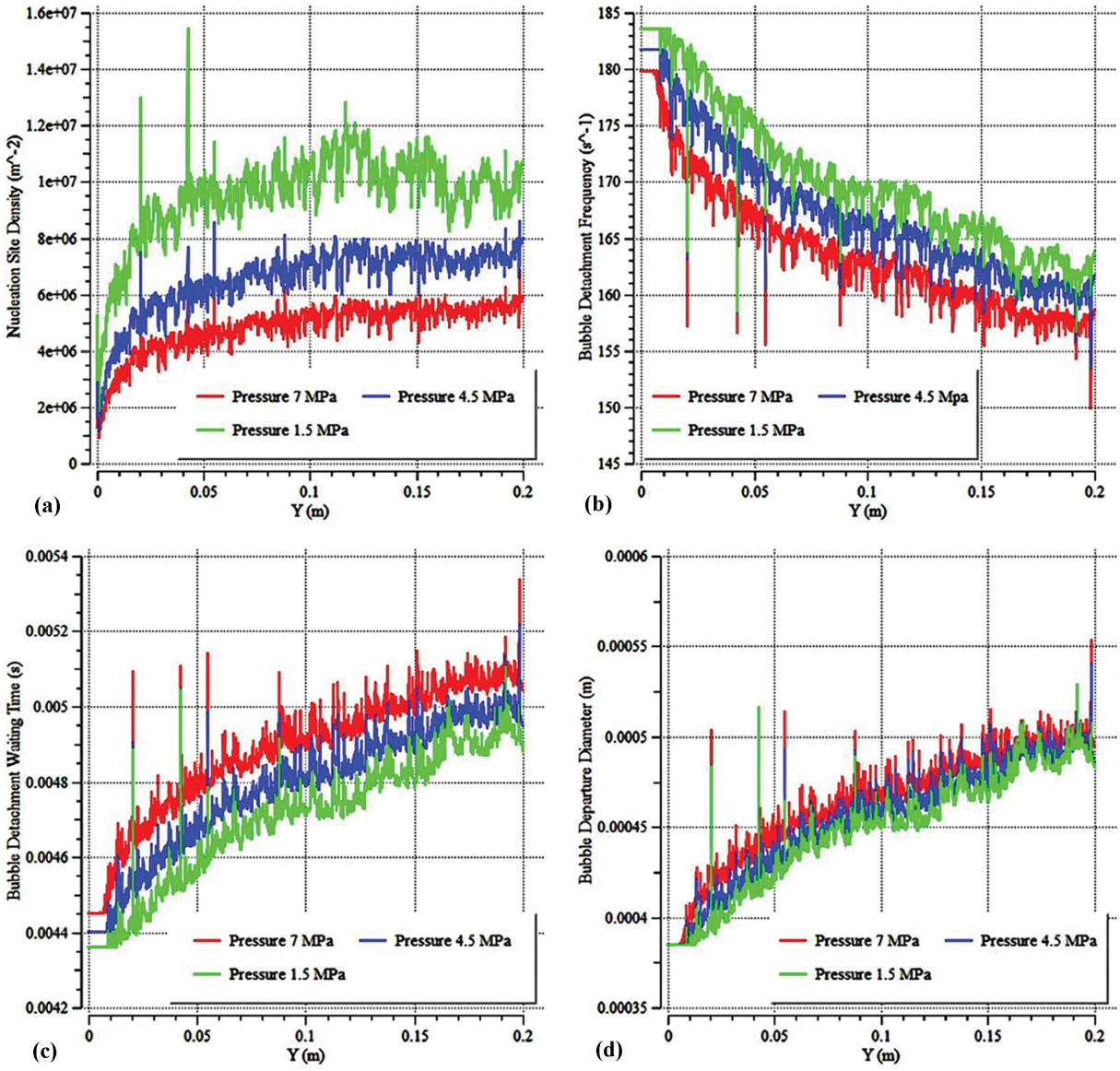

Fig. 7. Effect of pressure on bubble dynamics (a) nucleation site density, (b) bubble detachment frequency, (c) bubble detachment waiting time, (d) bubble departure diameter.

7 MPa are 39 K, 35 K, and 31 K, respectively. The superheat temperature for 1.5 MPa is higher than the other two. Therefore, it is expected that its nucleation site density should be more than the other two pressures.

Fig. 7 shows that the bubble detachment frequency decreases with the increment of pressure, while the bubble detachment waiting time and bubble departure diameter increase with pressure. The pressure influences the surface temperature, saturation temperature, and bulk fluid temperature, which changes the bubble behavior, as discussed earlier. The difference between the saturation temperature and bulk fluid temperature decreases with increasing pressure, which enhances the bubble departure diameter. The bubble detachment frequency decreases when the bubble departure diameter increases, increasing the bubble waiting time as well.

In fluid mechanics, the velocity is decreased by increasing the pressure, as it reduces the vortexes and turbulence. It applies to the rough surface walls on the micron scale. The turbulence near the wall surface is decreased due to the pressure increase, which leads to a decrease in the bubble detachment velocity. This leads to the lower bubble detachment frequency and higher waiting time and bubble departure diameter. In Fig. 7(a) the nucleation site density is decreased due to the increase of the pressure, and so the number of bubbles formed on the wall surface is decreased. While the number of bubbles is decreased, the heat flux is applied to the lower number of the bubbles, which leads to a higher departure diameter, as shown in Fig. 7(b)-(d). According to Zhou et al. [49], increasing the pressure in a specific heat flux leads to a decrease in the values of surface temperature. This reduction in the values of sur-

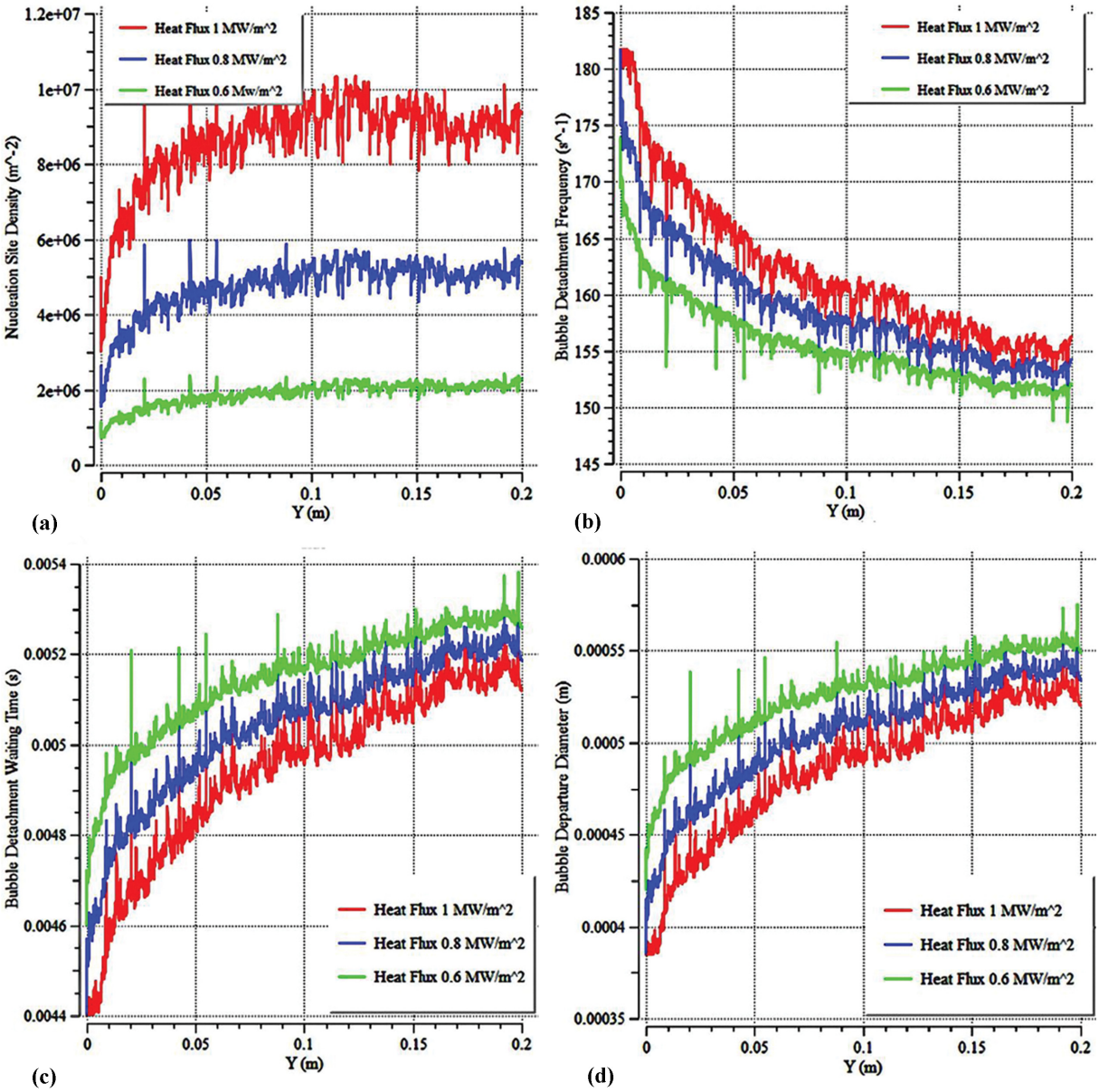

Fig. 8. Heat flux effects on bubble dynamics (a) nucleation site density, (b) bubble detachment frequency, (c) bubble detachment waiting time, (d) bubble departure diameter.

face temperature, causes the number of nucleation sites to decrease.

3. Heat Flux Effects on Bubble Dynamics Using DRS

Fig. 8 shows heat flux effects on bubble properties for the pressure of 4.5 MPa, mass flux of 600 kg/m^{2}s, and subcooled temperature of 5 K. In Fig. 8(a), nucleation site density is increased with increasing heat flux due to an increment in the superheat temperature caused by an increase in the wall surface temperature. As the pressure is constant, the saturation temperature also remains constant, so as wall surface temperature increases, superheat temperature also is increased, and consequently, nucleation site density is increased. Fig. 8(b) shows that the bubble detachment frequency increases with the rise in the heat flux. The heat momentum to the bubbles is increased by increasing the heat flux, which causes turbulence near the walls. The higher turbulence near the wall leads to the higher bubble departure velocity, which means the higher detachment frequency.

Fig. 8(c) shows that the bubble detachment waiting time decreases by the increment of the heat flux due to an increase in the bubble detachment frequency. Fig. 8(d) shows that the bubble departure diameter is decreased by increasing the heat flux. This is due to the increase and decrease in bubble detachment frequency and bubble detachment waiting time, respectively. As the bubbles are formed faster, by increasing heat flux, they have less time to grow; therefore, the bubble departure diameter increases.

The waiting time, bubble detachment frequency, and bubble departure diameter are closely dependent on each other. So, in Fig. 8, the surface temperature is increased by the increase of the heat flux, and it is an essential factor resulting in the increase of the

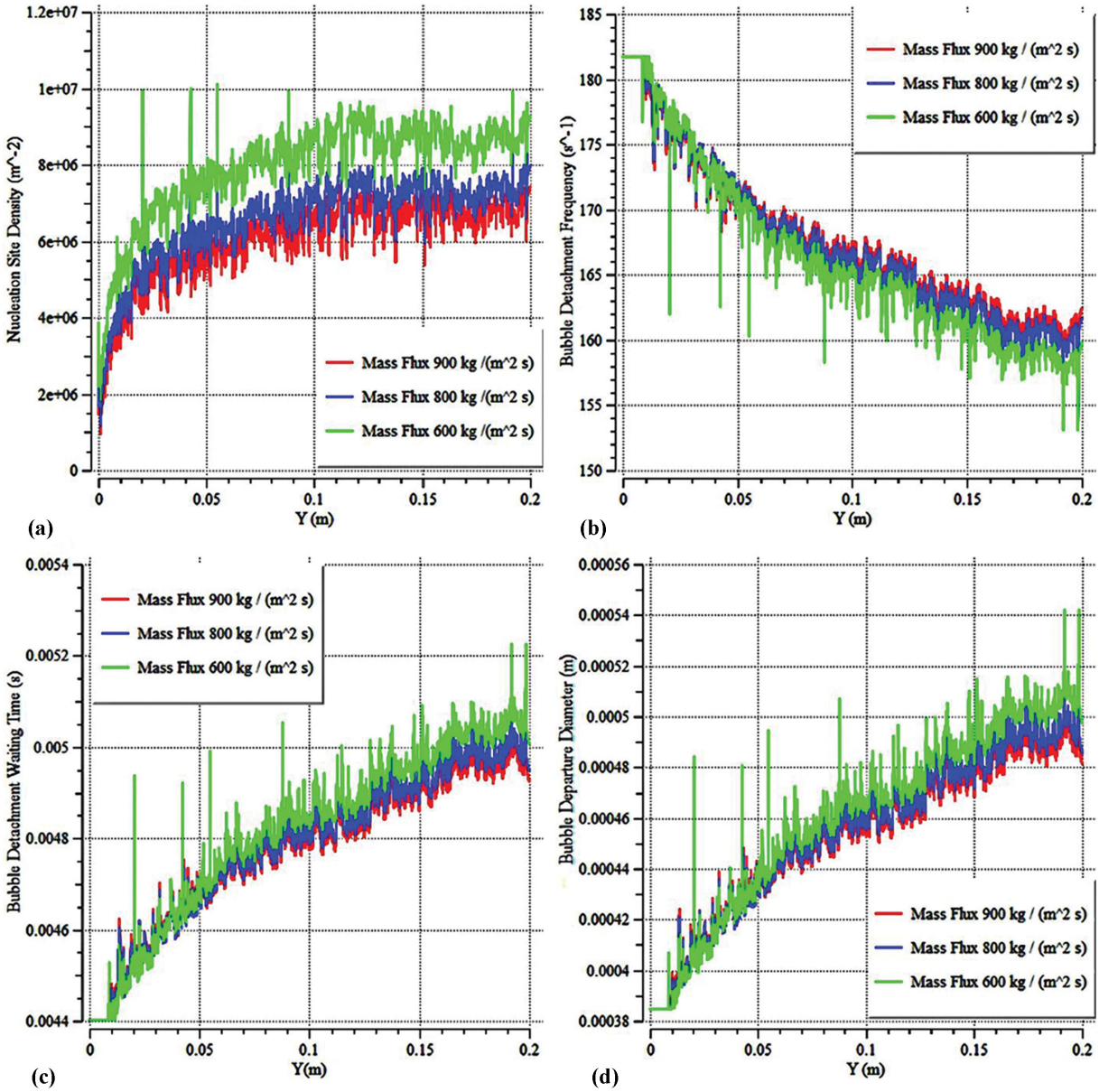

Fig. 9. Mass flux effects on bubble dynamics (a) nucleation site density, (b) bubble detachment frequency, (c) bubble detachment waiting time, (d) bubble departure diameter.

active nucleation site density. While the nucleation site density is increased, more bubbles are formed on the surface. Fig. 8(a) shows that the nucleation site density is increased four-fold by increasing the heat flux from 0.6 MW/m^2 to 0.8 MW/m^2. So, the number of bubbles formed on the surface is increased proportionally. Therefore, the bubbles receive less heat in the higher heat fluxes compared to the lower heat fluxes, which leads to their lower diameter and higher detachment frequency. In the higher heat fluxes, the distance between bubbles is decreased, and the detachment velocity is increased. It leads to the merging of the two or more bubbles (bubble coalescence) and forming a bulk of the bubbles that shows the detached flow from the surface as a slug. Ren et al. [50] showed that nucleation sites increased when the heat flux went up. The experimental findings of Ren et al. [50] follow the same trend as the present numerical study.

4. Mass Flux Effects on Bubble Dynamics Using DRS

The effects of mass flux on bubble properties for flow boiling are illstrated in Fig. 9. The pressure is 4.5 MPa, heat flux is 1 MW/m^2, and subcooled temperature is 10 K. Based on Fig. 9(a), nucleation site density is decreased by the increment of the mass flux. The role of the latent heat of vaporization in heat transfer of flow boiling is equal for all mass fluxes, but for lower mass fluxes, it has a direct effect on the nucleation site. As a consequence, more nucleation sites are generated for lower mass flux, which leads to an increment in nucleation site density. Ren et al. [50] and Zhou et al. [49] found similar results that nucleation site density is reduced by increasing the mass flow rate.

In Fig. 9(b), mass flux does not have a considerable effect on

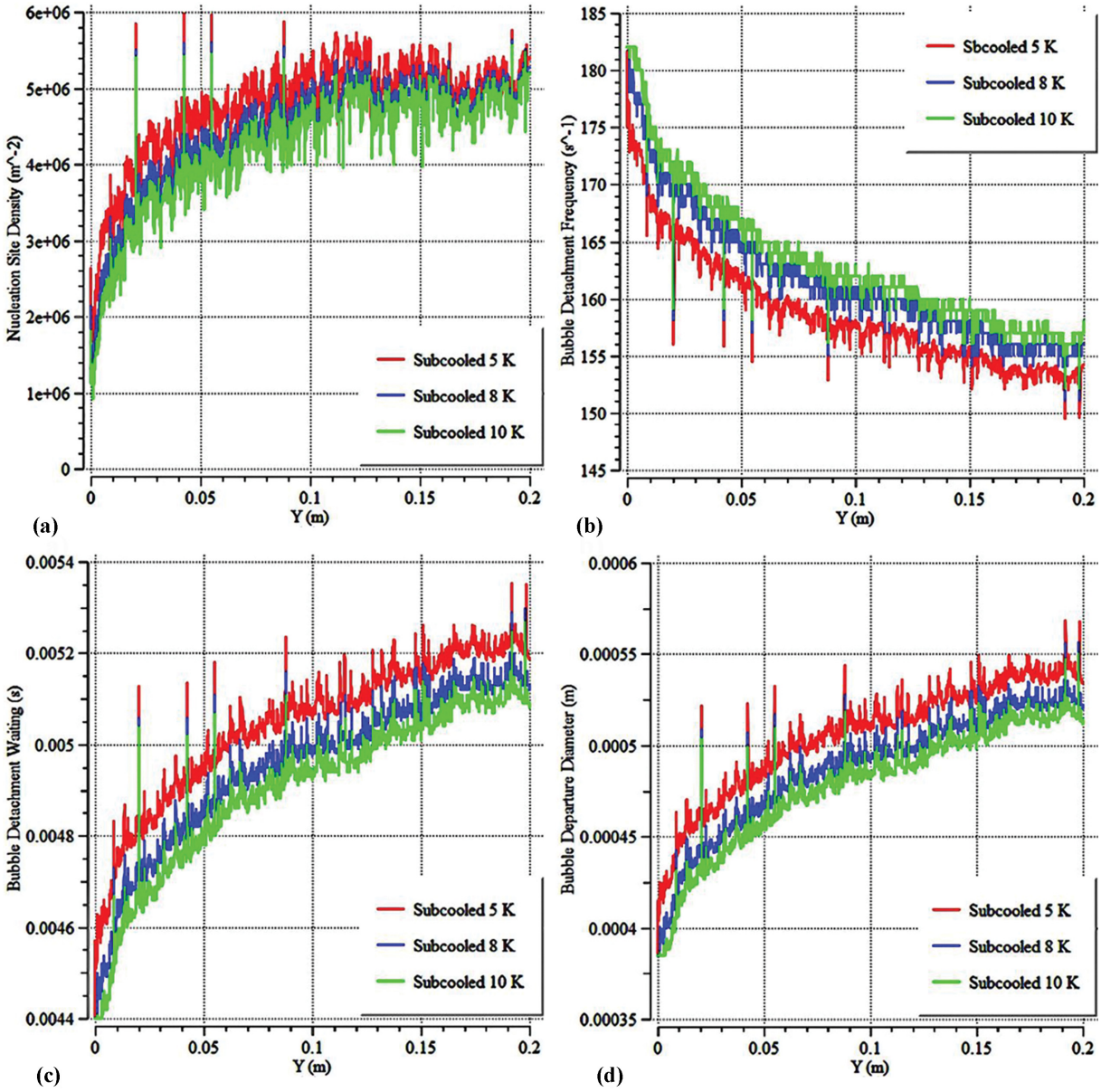

Fig. 10. Subcooled temperature effects on bubble dynamics (a) the nucleation site density, (b) the bubble detachment frequency, (c) the bubble detachment waiting time, (d) the bubble departure diameter.

bubble detachment frequency. However, bubble detachment frequency is slightly increased by the increment of mass flux.

In Fig. 9(c), mass flux does not have a considerable effect on bubble detachment waiting time. However, waiting time for bubble detachment is increased by decreasing mass flux. This happens due to the decrease of the velocity gradient in nearby the wall. Sarker et al. [47] indicated that bubble waiting time was slightly reduced when the mass flux increased, which is an indicator that the results of the present numerical modeling followed the same trend as the experimental findings of Sarker et al. [47].

Based on Fig. 9(d), the bubble departure diameter decreases slightly by the increment of the mass flux. The velocity gradient near the wall is increased by increasing mass flux, which leads to a decrease in the bubble detachment waiting. Therefore, less time is available for increasing bubble departure diameter, which leads to the detachment of bubbles with smaller diameters. According to Sarker et al. [47], bubble departure diameter decreased when the liquid velocity increased. Sugrue et al. [51], as well as Rousselet [52], also found similar results when they investigated the impact of increasing the mass flux on the bubble departure diameter. Also, decreasing the bubble departure leads to increase in bubble detachment frequency.

5. Subcooled Temperature Effects on Bubble Dynamics Using DRS

The effects of subcooled temperature on bubble properties for flow boiling are studied in Fig. 10. The heat flux, pressure, and mass flux are 0.8 MW/m^2, 4.5 MPa, and 600 kg/m^2s, respectively. Fig. 10(a) shows that the nucleation site density is decreased slightly by increasing subcooled temperature. This happens due to a small change of wall surface temperature that has a direct effect on nucleation site density. According to Zohu et al. [49], Ren et al. [50], and Lie and Lin [53], nucleation site density decreases when the subcooled temperature rises. This shows that the present numerical study followed the same trend as the experimental results.

Fig. 10(b) shows that the bubble detachment frequency is enhanced by increasing subcooled temperature. The increase of subcooled temperature leads to a decrease in bulk fluid temperature, which causes a reduction of bubble departure diameter. Bubble detachment frequency and bubble departure diameter have an inverse relationship, so bubble detachment frequency is increased by the increase of subcooled temperature. Fig. 10(c) illustrates that bubble detachment waiting is decreased by the increase of subcooled temperature due to an increase in the frequency of detachment. The increase of bubble detachment frequency leads to the faster departure of bubbles and decrease of bubble detachment waiting.

In Fig. 10(d), bubble departure diameter is decreased by enhancing subcooled temperature. Increasing subcooled temperature leads to a decrease in bulk fluid temperature and finally causes a decrease of bubble departure diameter. Enhancing bubble detachment frequency and decrease of bubble detachment waiting time leads to a decrease of bubble departure diameter.

CONCLUSIONS

A numerical scheme for the random surface roughness simulation was designed in subcooled flow boiling. The vapor and liquid phase interaction was considered by exerting the Euler-Euler method. Surface roughness was simulated by a surface roughness model (SRM) and a direct roughness simulation (DRS). The DRS was used to generate and simulate roughness heights randomly. Here, the surface roughness effects on the bubble dynamics were studied using DRS. The results with those of the SRM and smooth surface (SS) were compared. The following conclusions were made:

- The nucleation site density decreases when using the SRM and the DRS as compared to those of the SS. The reduction in the nucleation site density at outlet was 28.05% for the DRS and 25.5% for the SRM compared to SS.
- Compared to the SS, the bubble detachment frequency at oulet 2.04% decreased when using the SRM and 6.5% increased when using the DRS.
- Compared to the SS, the bubble departure diameter at outlet 4.3% increased when using the SRM and 11.8% decreased when using the DRS.
- Compared to the SS, the bubble detachment waiting time at outlet 2% increased when using the SRM, and 6.08% decreased when using the DRS.
- The DRS has the following effects on the nucleation bubble.

The increase of pressure leads to a decrease of the nucleation site density and bubble detachment frequency, but causes an increase of the bubble detachment waiting time and the bubble departure diameter.

Increasing heat flux leads to the increase of the nucleation site density and the bubble detachment frequency, while causing a decrease in the bubble detachment waiting time and the bubble departure diameter.

Increasing mass flux causes to decrease the nucleation site density, the bubble detachment frequency, and the bubble departure diameter, while causing an increase of bubble detachment waiting time. Note that these effects are very low.

The increase of subcooled temperature leads to the decrease of the nucleation site density, the bubble detachment waiting time, and the bubble departure diameter, while causing an increase of the bubble detachment frequency.

REFERENCES

1. A. Bozorgnezhad, M. Shams, G. Ahmadi, H. Kanani and M. Hasheminasab, *The experimental study of water accumulation in PEMFC cathode channel* (2015).
2. M. Hasheminasab, A. Bozorgnezhad, M. Shams, G. Ahmadi and H. Kanani, *Simultaneous investigation of PEMFC performance and water content at different flow rates and relative humidities* (2014).
3. A. Bozorgnezhad, M. Shams, H. Kanani and M. Hasheminasab, *J. Dispers. Sci. Technol.*, **36**, 1190 (2015).
4. T. Hibiki and M. Ishii, *J. Comput. Multiph. Flows*, **1**, 1 (2009).
5. J. F. F. Klausner, R. Mei, D. M. M. Bernhard and L. Z. Z. Zeng, *Int. J. Heat Mass Transf.*, **36**, 651 (1993).
6. G. E. Thorncroft, J. F. Klausnera and R. Mei, *Int. J. Heat Mass Transf.*, **41**, 3857 (1998).
7. C. S. Brooks, B. Ozar, T. Hibiki and M. Ishii, *Nucl. Eng. Des.*, **268**, 152 (2014).

8. H. Alimoradi, M. Shams, N. Ashgriz and A. Bozorgnezhad, *Case Stud. Therm. Eng.*, **24**, 100829 (2021).
9. D. Prabhudharwadkar, M. A. Lopez de Bertodano, J. Buchanan, Jr. and A. Vaidheeswaran, *In International Heat Transfer Conference*, **49361**, 655 (2010).
10. M. Ishii and T. Hibiki, *Thermo-fluid dynamics of two-phase flow*, Springer Science & Business Media (2010).
11. M. Jakob and SP. Kezios, *Heat Transfer.*, **2** (1949).
12. B. B. Mikic, W. M. Rohsenow and P. Griffith, *Int. J. Heat Mass Transf.*, **13**, 657 (1970).
13. Y. Y. Hsu and R. W. *Graham, Transport processes in boiling and two-phase systems, including near-critical fluids*, Hemisphere Pub. Corp., Washington (1976).
14. R. F. Gaertner and J. W. Westwater, *Chem. Eng. Prog.*, **56**, 39 (1960).
15. S. R. R. Yang and R. H. H. Kim, *Int. J. Heat Mass Transf.*, **31**, 1127 (1988).
16. G. Kocamustafaogullari and M. Ishii, *Int. J. Heat Mass Transf.*, **26**, 1377 (1983).
17. T. Hibiki and M. Ishii, *Int. J. Heat Mass Transf.*, **46**, 2587 (2003).
18. N. Basu, G. R. Warrier and V. K. Dhir, *J. Heat Transfer*, **124**, 717 (2002).
19. C. S. Brooks, N. Silin, T. Hibiki and M. Ishii, *J. Heat Transfer*, **5**, 137 (2015).
20. A. Parahovnik and Y. Peles, *Int. J. Heat Mass Transf.*, **183**, 122191 (2022).
21. J. Bhati and S. Paruya, *Nucl. Eng. Des.*, **371**, 110945 (2021).
22. A. Mukherjee, D. N. Basu and P. K. Mondal, *Int. J. Multiph. Flow*, **148**, 103923 (2022).
23. A. Khoshnevis, A. Sarchami and N. Ashgriz, *Appl. Therm. Eng.*, **135**, 280 (2018).
24. H. Alimoradi and M. Shams, *Appl. Therm. Eng.*, **111**, 1039 (2017).
25. H. Alimoradi, M. Shams and Z. Valizadeh, *Modares Mech. Eng.*, **16**, 545 (2017).
26. M. H. Zolfagharnasab, M. Salimi, H. Zolfagharnasab, H. Alimoradi, M. Shams and C. Aghanajafi, *Powder Technol.*, **380**, 1 (2021).
27. H. Alimoradi and M. Shams, *Modares Mech. Eng.*, **19**, 1613 (2019).
28. M. Roodbari, H. Alimoradi, M. Shams and C. Aghanajafi, *J. Therm. Anal. Calorim.*, **147**(4), 3283 (2022).
29. H. Alimoradi, S. Zaboli and M. Shams, *Korean J. Chem. Eng.*, **39**, 69 (2022).
30. S. Zaboli, H. Alimoradi and M. Shams, *J. Therm. Anal. Calorim.*, **147**, 1 (2022).
31. A. Chen, T. F. Lin, H. M. Ali and W.-M. Yan, *Int. J. Heat Mass Transf.*, **157**, 119974 (2020).
32. H. I. Mohammed and D. Giddings, *Int. J. Therm. Sci.*, **146**, 106099 (2019).
33. H. I. Mohammed, D. Giddings and G. S. Walker, *Int. J. Heat Mass Transf.*, **125**, 218 (2018).
34. H. I. Mohammed, D. Giddings and G. S. Walker, *Int. J. Heat Mass Transf.*, **130**, 710 (2019).
35. H. I. Mohammed, D. Giddings and G. S. Walker, *Int. J. Heat Mass Transf.*, **134**, 1159 (2019).
36. M. Lemmert and J. M. Chawla, *Heat Transf. Boil.*, **237**, 247 (1977).
37. R. Cole, *AIChE J.*, **6**, 533 (1960).
38. V. I. Tolubinsky and D. M. Kostanchuk, *in International Heat Transfer Conference*, **23**, 4 (1970).
39. N. Kurul and Z. Michael, Podowski. In International Heat Transfer Conference Digital Library (1990).
40. E. Krepper and R. Rzehak, *Nucl. Eng. Des.*, **241**, 3851 (2011).
41. E. Krepper, R. Rzehak, C. Lifante and T. Frank, *Nucl. Eng. Des.*, **255**, 330 (2013).
42. E. Krepper, B. Končar and Y. Egorov, *Nucl. Eng. Des.*, **237**, 716 (2007).
43. G. G. Bartolomei, V. G. Brantov, Y. S. Molochnikov, Y. V. Kharitonov, V. A. Solodkii, G. N. Batashova and V. N. Mikjailov, *Therm. Eng.*, **29**, 132 (1982).
44. F. M. White and J. Majdalani, *Viscous fluid flow*, vol. 3. McGraw-Hill New York (2006).
45. H. Schlichting and K. Gersten, *Boundary-layer theory*, Springer (2016).
46. H. Setoodeh, A. Keshavarz, A. Ghasemian and A. Nasouhi, *Appl. Therm. Eng.*, **90**, 384 (2015).
47. D. Sarker, W. Ding, C. Schneider and U. Hampel, *Int. J. Heat Mass Transf.*, **142**, 118481 (2019).
48. J. P. McHale and S. V Garimella, *Exp. Therm. Fluid Sci.*, **44**, 439 (2013).
49. P. Zhou, R. Huang, S. Huang, Y. Zhang and X. Rao, *Int. J. Heat Mass Transf.*, **149**, 119105 (2020).
50. T. Ren, Z. Zhu, M. Yan, J. Shi and C. Yan, *Int. J. Heat Mass Transf.*, **144**, 118670 (2019).
51. R. Sugrue, J. Buongiorno and T. McKrell, *Nucl. Eng. Des.*, **279**, 182 (2014).
52. Y. L. Rousselet, *Interacting effects of inertia and gravity on bubble dynamics*, University of California, Los Angeles (2014).
53. Y. M. Lie and T. F. Lin, *Int. J. Heat Mass Transf.*, **49**, 2077 (2006).